Supporting Information

Melanin: A Greener Route to Enhance Energy Storage under Solar Light

Ri Xu[a], Abdelaziz Gouda[a*], Maria Federica Caso[b], Francesca Soavi[c**] and Clara Santato[a**]*

[a]Department of Engineering Physics, Polytechnique Montréal, C.P. 6079, Succ. Centre-ville, Montréal, QC, H3C 3A7, Canada

[b] Nanofaber Spin-Off at ENEA, Casaccia Research Centre, Via Anguillarese 301, Roma, 00123, Italy

[c]Dipartimento di Chimica "Giacomo Ciamician", Alma Mater Studiorum Università di Bologna, Via Selmi, 2, 40126 Bologna, Italy

[*] Authors contributed equally to this work.

**Correspondence and requests for materials should be addressed to C.S. and F.S. (e-mail: clara.santato@polymtl.ca and francesca.soavi@unibo.it)

Cyclic voltammetry on carbon paper

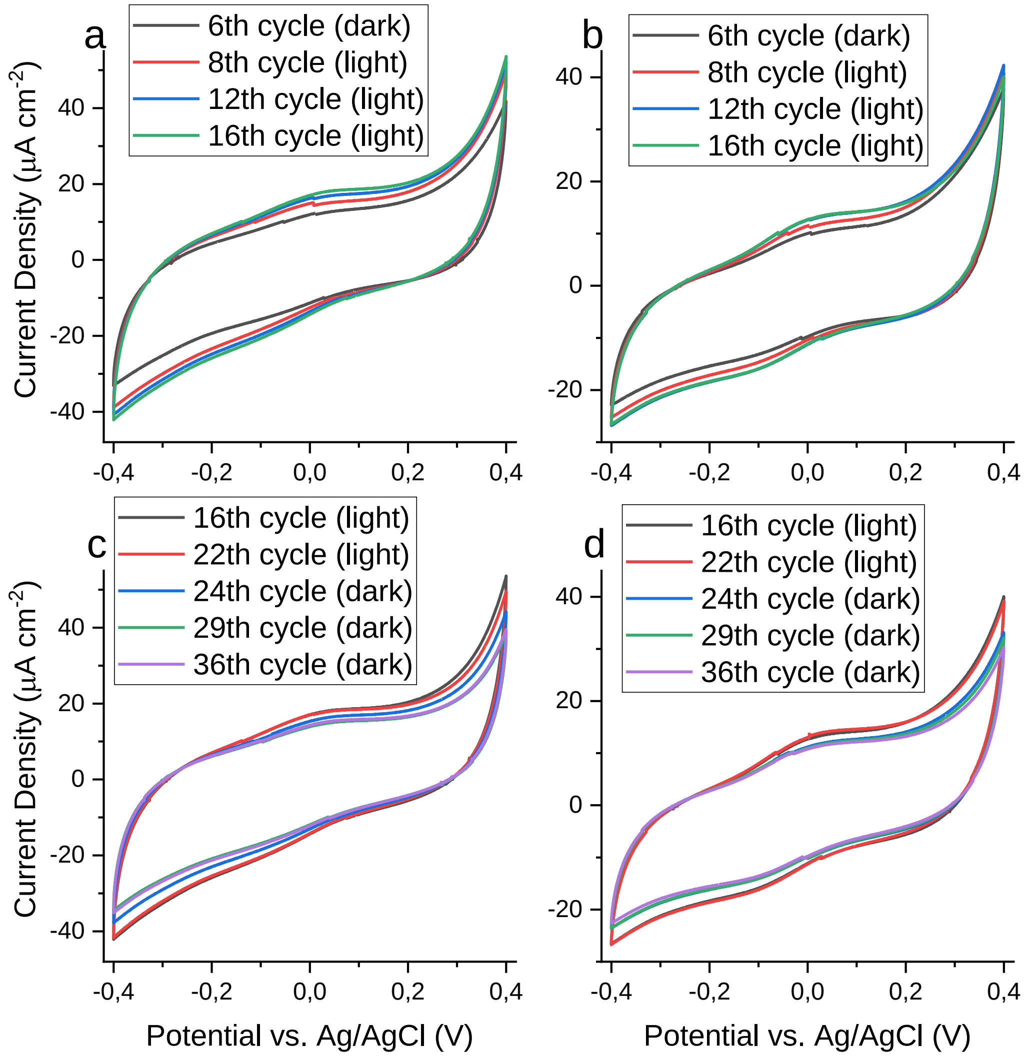

Figure S1. Cyclic voltammetry of (a, c) DHI-melanin and (b, d) DHI/DHICA-melanin on carbon paper electrodes (loading 0.1 mg/cm^2) at 5 mV/s. Protocol of acquisition: dark (6 cycles) → light (16 cycles) → dark (14 cycles).

Under light irradiation, the current for both melanins slightly increases. Table S2 includes the values of the capacity and capacitance, for dark and light conditions, for increasing cycle numbers.

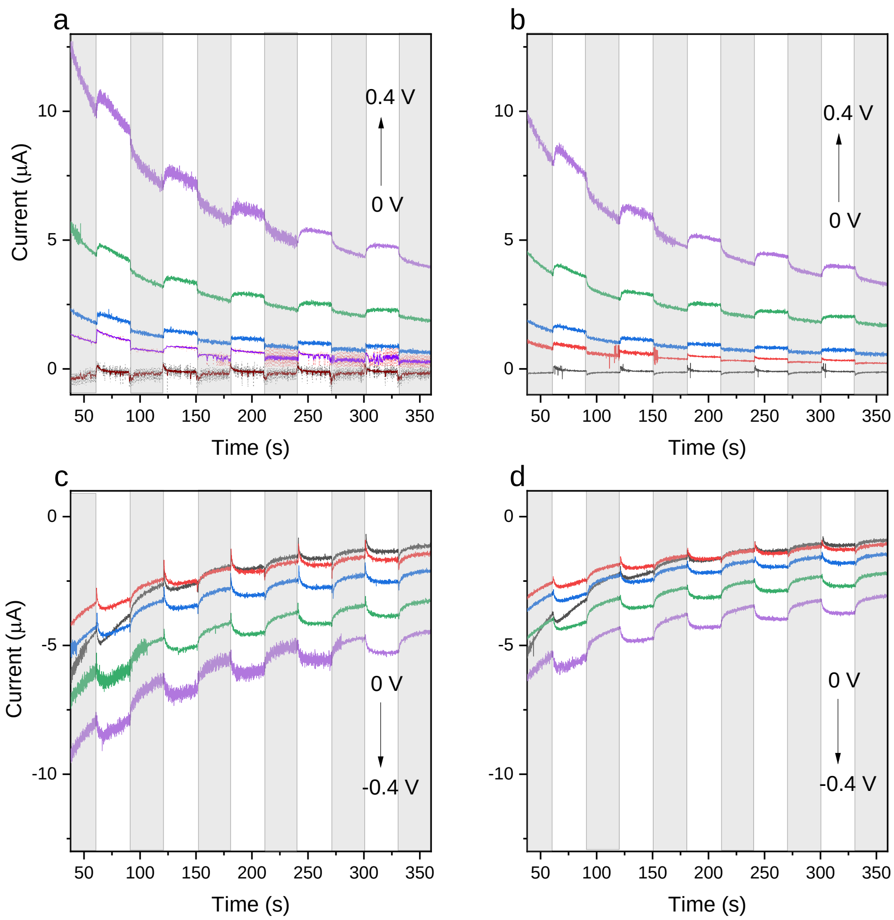

Figure S2. Current measurements with chopped light for (a) (c) DHI-melanin and (b) (d) DHI/DHICA-melanin. Gray rectangles represent the lapse of time spent by the samples in the dark. Acquisition protocol: 0 V → 0.1 V → 0.2 V→ 0.3 V → 0.4 V → 0 V → -0.1 V → -0.2 V → -0.3 V → -0.4 V vs Ag/AgCl. Prior the current measurements, fresh electrodes were pre-cycled in the potential range -0.4 V/0.4 V, at 5 mV/s, for 5 cycles. Current measurements carried out on DHI- and DHI/DHICA-melanins indicate an increase of the current under light conditions, for both anodic and cathodic applied potentials.

Considering the more significant effect of the light on the current when a positive potential is applied to the photoelectrode, a positive potential has been used throughout this work to study the effect of the light on the electrochemical energy storage performance of melanin electrodes. Work is in progress to study, by time resolved spectroscopy and DFT calculations, the reasons why the positive potential induces a superior effect on the current with respect to the negative potential.

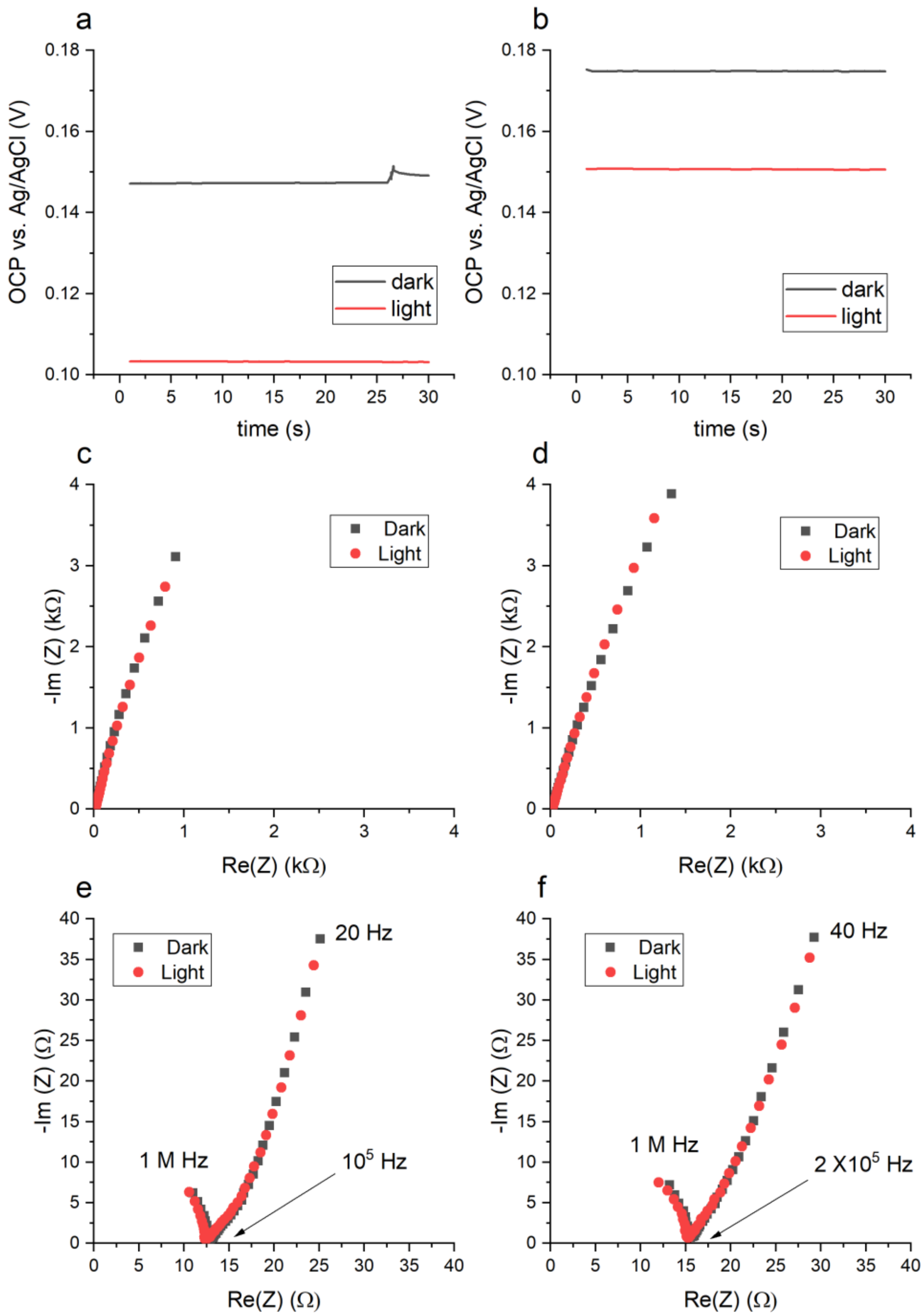

Figure S3. Open circuit potential measurements of (a) DHI-melanin and (b) DHI/DHICA-melanin. Nyquist plots at frequency range 10^6 Hz-10^{-1} Hz of (c) DHI-melanin and (d) DHI/DHICA-melanin. (e) and (f) are zoomed high-frequency-range Nyquist plots for DHI-melanin and DHI/DHICA-melanin, respectively. Acquisition protocol: Open circuit potential vs. time (dark) → EIS (dark) → 40 min irradiation (without bias) → open circuit potential vs. time (light) → EIS (light).

Bare carbon paper

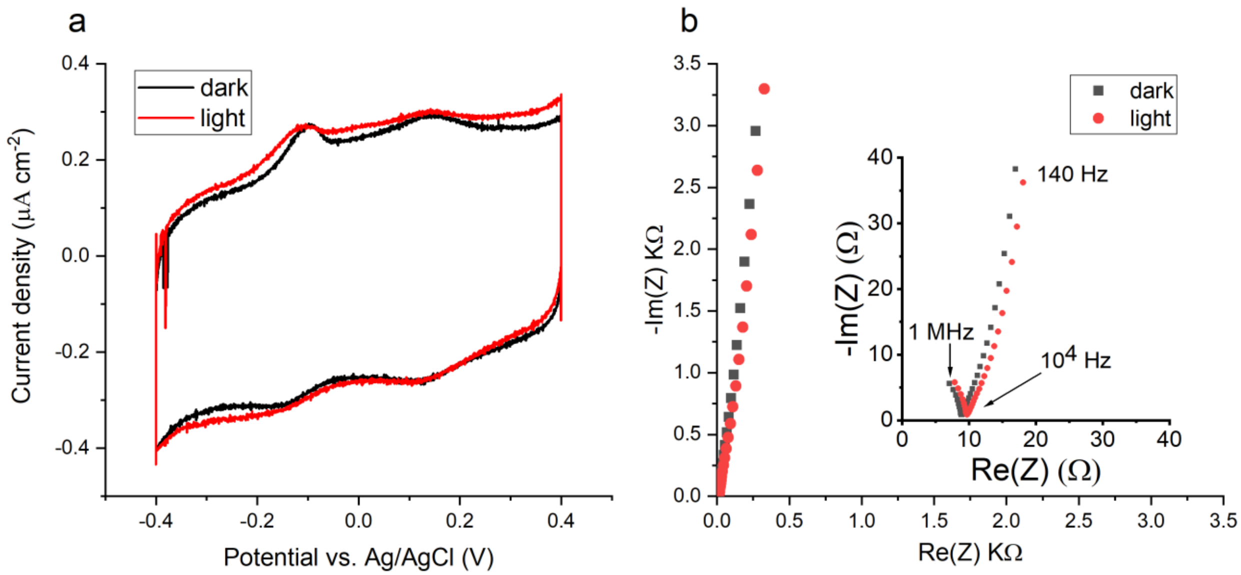

Figure S4. (a) Cyclic voltammetry at 5 mV/s and (b) Nyquist plot of bare carbon paper (inset: high frequency), 0.25 M $NaCH_3COO$ (pH 5).

Galvanostatic charge-discharge measurements

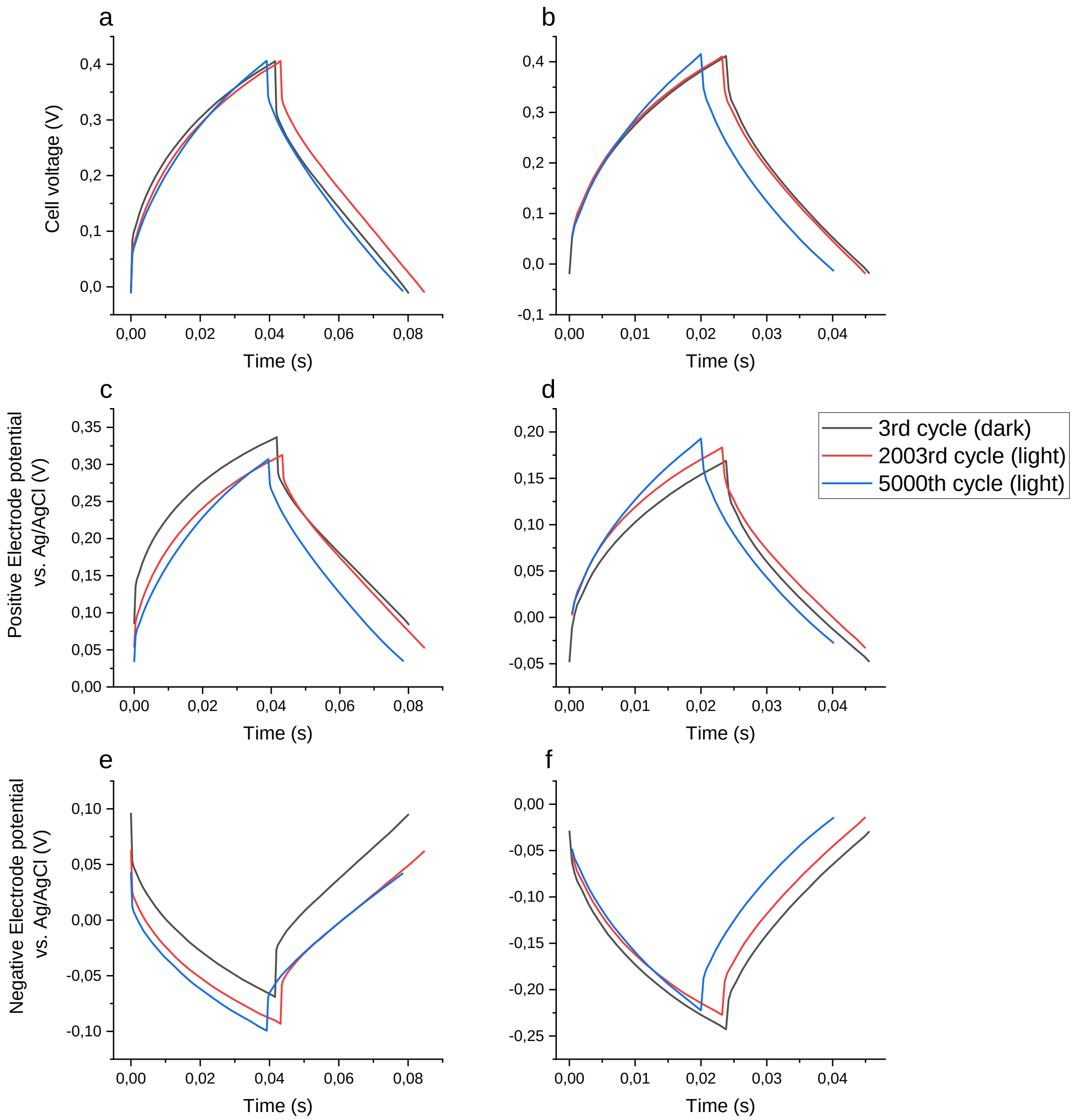

Figure S5. Galvanostatic curves of DHI-melanin (a, c, e) and DHI/DHICA-melanin (b, d, f). Black: 3rd cycle (under dark). Red: 2003rd cycle (under light, after 40 min irradiation). Blue: 5000th cycle (last cycle, under light conditions). Protocol of acquisition: dark → light → 40 min irradiation (without bias) light → dark → light, each for 1000 cycles.

Figure S5 shows 3 cycles of galvanostatic curves. Under light conditions, the potentials of both positively and negatively biased DHI-melanin electrodes shift towards negative values, by ca 9% (from 0.34 in the 3rd cycle to 0.31 V in both 2003rd cycle and 5000th cycle), whereas for DHI/DHICA-melanin shift towards positive values, by 6% (from 0.17 in the 3rd cycle to 0.18 V in 2003rd cycle) and 12% (from 0.17 in the 3rd cycle to 0.19 V in the 5000th cycle).

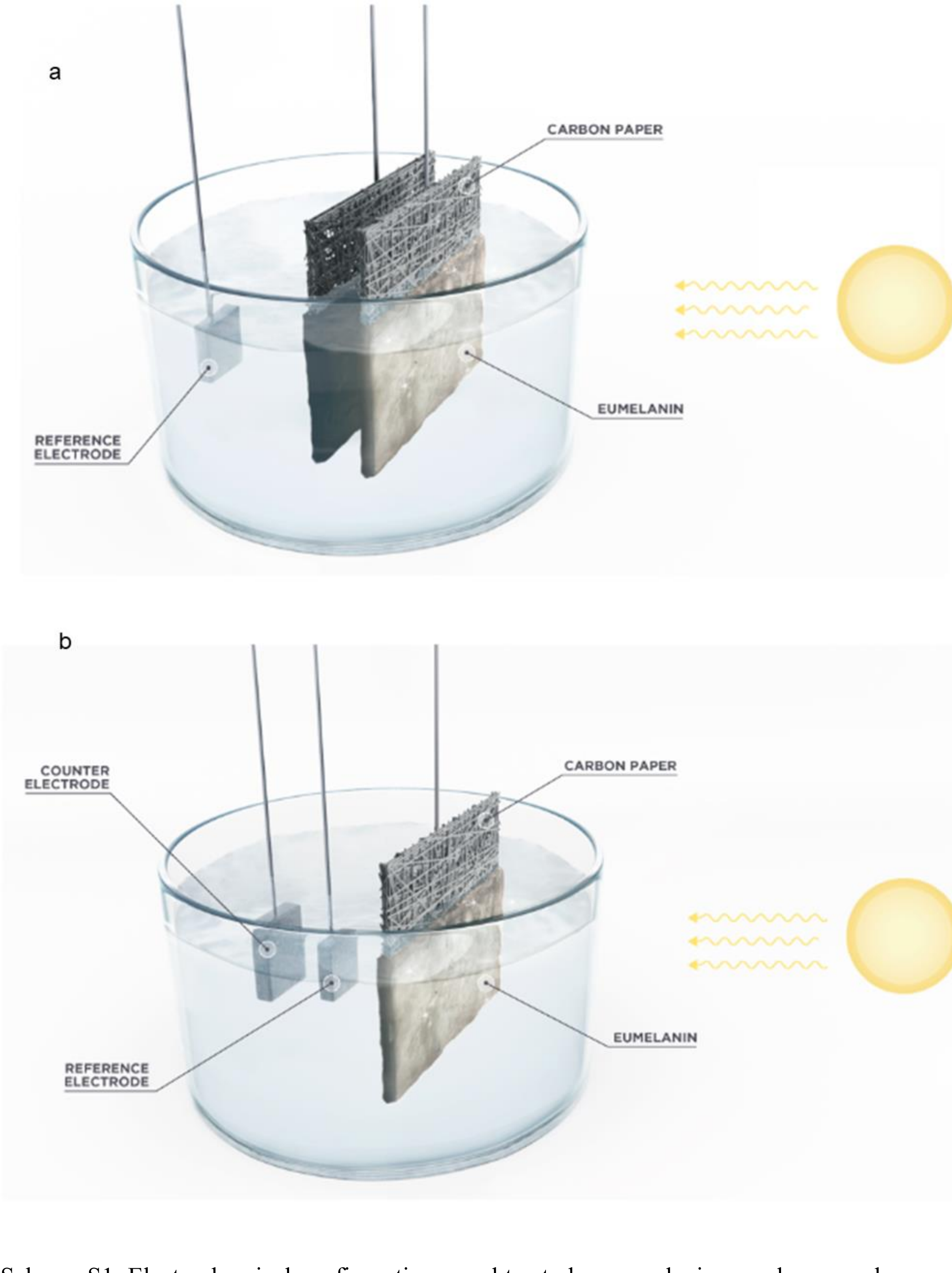

Scheme S1. Electrochemical configurations used to study our melanin samples on carbon paper: (a) supercapacitor (including a reference electrode) and (b) single electrode.

Table S1. Performance of integrated solar cells and energy storage devices in the literature (see explanations of abbreviations and acronyms below).

Device structure	Electrode materials	Electrolyte	Energy storage performance	Efficiency (%)	Ref
PSB*	$M_{an\text{-}ph}$* WO_3/TiO_2/N719* $M_{ce\text{-}ph}$ Pt	EL_{ph}* LiI/I_2/PC*/tBP*	Q_{ch}* 1.8 C cm^{-2}	η_{tot} 0.6	1
DSSC*/SC*	$M_{an\text{-}ph}$ TiO_2/N719 $M_{ce\text{-}ph}$ Pt M_{ES+}, M_{ES-} PEDOT	EL_{ph} LiI/I_2/tert-butyl alcohol/tBP EL_{ES}* $LiClO_4$/MPN*	C_s* 0.52 F cm^{-2}	η_{con} 4.4	2
DSSC/SC	$M_{an\text{-}ph}$ TiO_2/N3 $M_{ce\text{-}ph}$ Pt M_{ES+}, M_{ES-} PProDOT-Et_2*	EL_{ph} LiI/I_2/CH_3CN EL_{ES} $LiClO_4$/MPN	C_s 0.48 F cm^{-2} E_{max}* 22 Wh cm^{-2} P_{max}* 0.6 mW cm^{-2}	η_{stor} 0.6	3
DSSC/SC (1D)	$M_{an\text{-}ph}$ ZnO NW/N719 $M_{ce\text{-}ph}$ ZnO NW/graphene M_{ES+}, M_{ES-} ZnO NW	EL_{ph} LiI/I_2/tBP/MPN EL_{ES} PVA/H_3PO_4 gel	C_s 0.4 mF cm^{-2}	η_{con} 0.02	4
OPV*/SC	$M_{an\text{-}ph}$ P3HT/PCBM* $M_{ce\text{-}ph}$ Al M_{ES+}, M_{ES-} CNT	EL_{ph} PEDOT/PSS EL_{ES} PVA/H_3PO_4 gel	C_s 28 F g^{-1}	η_{con} 3.4	5
DSSC/SC (1D)	$M_{an\text{-}ph}$ Ti/TiO_2/N719 $M_{ce\text{-}ph}$ CNT M_{ES-} Ti/TiO_2 M_{ES+} CNT	EL_{ph} LiI/I_2/DMPII*/tBP/ CH_3CN EL_{ES} PVA/H_3PO_4 gel	C_s 0.6 mF cm^{-2}	η_{stor} 68 η_{tot} 1.5	6
Tandem solar cell/LIB	$M_{an\text{-}ph}$ TiO_2 NT/N719 $M_{ce\text{-}ph}$ Pt M_{ES-} Ti/TiO_2 NT/N749 M_{ES+} $LiCoO_2$/carbon	EL_{ph} LiI/I_2/tBP/CH_3CN EL_{ES} $LiPF_6$/ethylene carbonate/dimethyl carbonate	Q_{dis}* 39 µAh	η_{tot} 0.82	7
DSSC/SC	$M_{an\text{-}ph}$ TiO_2/N719 $M_{ce\text{-}ph}$ ZnO NW/PVDF M_{SC+} Pt/Au M_{SC-} ZnO NW/PVDF	EL_{ph} LiI/LiI_3/GNCS* /DMII*/tBP/MPN/ CH_3CN	Q_{dis} 2.1 C g^{-1}	η_{con} 3.7	8

DSSC/RFB*	$M_{an\text{-}ph}$ m-TiO_2/Z907* $M_{ce\text{-}ph}$ Pt M_{ES+}, M_{ES-} Pt	EL_{ca} LiI/I_2/$LiClO_4$/PC EL_{an} DMFc*/$LiClO_4$/MPN **for both DSSC and RFB**	Q_{dis} 53 mAh l^{-1}	η_{con} 0.15	9
DSSC/SC (1D)	$M_{an\text{-}ph}$ TiO_2/N719 $M_{ce\text{-}ph}$ PaNi M_{ES+}, M_{ES-} PaNi	EL_{ph} BmimI*/I_2/tBP/$LiClO_4$/GITC*/CH_3CN EL_{ES} H_2SO_4	C_s 41 mF cm^{-2}	η_{tot} 2.1 η_{con} 5.4	10
DSSC/SC	$M_{an\text{-}ph}$ TiO_2/N719 $M_{ce\text{-}ph}$ CNT/PaNi M_{ES+}, M_{ES-} CNT/PaNi	EL_{ph} LiI/I_2/tBP/DMPII/PVDF-co-HFP*/MPN EL_{ES} PVA/H_3PO_4 gel	C_s 208 F g^{-1}	η_{tot} 5.1 η_{con} 6.1	11
DSSC/SC	$M_{an\text{-}ph}$ TiO_2/N749 $M_{ce\text{-}ph}$ Pt M_{ES+}, M_{ES-} hydrogenated TiO_2	EL_{ph} LiI/I_2/tBP/DMPII/ MPN EL_{ES} Li_2SO_4	C_s 1.1 mF cm^{-2} C%* 99% @3000 cycles	η_{tot} 1.6 η_{con} 3.2	12
DSSC/SC (1D)	$M_{an\text{-}ph}$ TiO_2/N719 $M_{ce\text{-}ph}$ CNT M_{ES+}, M_{ES-} CNT	EL_{ph} LiI/I_2/tBP/DMPII/tBP/CH_3CN EL_{ES} PVA/H_3PO_4 gel	C_s 21.7 F g^{-1}	η_{tot} 1.8 η_{con} 6.5	13
Perovskite solar cell/LIB	$M_{an\text{-}ph}$ PC61BM* $M_{ca\text{-}ec}$ $LiFePO_4$ $M_{an\text{-}ec}$ $Li_4Ti_5O_{12}$	EL_{ph} $CHNH_3PbI_3$/PEDOT/ PSS EL_{ES} $LiFP_6$/ethylene carbonate/dimethyl carbonate/diethyl carbonate	Q_{dis} 142 mAh g^{-1}	η_{tot} 7.8 η_{con} 15.7	14
Perovskite Solar Cell/SC	$M_{an\text{-}ph}$ TiO_2 $M_{ce\text{-}ph}$ MoO_3/Au/MoO_3 M_{ES+}, M_{ES-} WO_3	EL_{ph} $CHNH_3PbI_{3\text{-}x}Cl_x$/spiro-MeOTAD* EL_{ES} PVA/H_2SO_4 gel	C_s 431 F m^{-2} E_{max} 25 mWh m^{-2} P_{max} 377 mW m^{-2}	η_{con} 11.9	15
Perovskite Solar Cell/SC	$M_{an\text{-}ph}$ c-TiO_2/nano TiO_2 $M_{ce\text{-}ph}$ PEDOT/carbon M_{ES+}, M_{ES-} PEDOT/carbon	EL_{ph} $CH_3NH_3PbI_3$ EL_{ES} $LiClO_4$/TMAI*/IPA*	C_s 12 mF cm^{-2} C% 95%@2000 cycles	η_{tot} 4.7 η_{con} 6.4 η_{stor} 74	16
SiNW solar cell/SC	$M_{an\text{-}ph}$ PEDOT/PSS /SiNW/n-doped Si $M_{ce\text{-}ph}$ Ag M_{ES+}, M_{ES-} polypyrrole	EL_{ph} PEDOT/PSS EL_{ES} PVA/H_3PO_4 gel	C_s 252 mF cm^{-2} E_{max} 8.8 μWh cm^{-2}	η_{tot} 10.5	17
Commercial solar cell/SC	M_{SC} Activated carbon/PVDF	EL_{ES} Na_2SO_4	C_s 170 Fg^{-1} C% 85% @15000 cycles	—	18

			E_{max} 17.7 Wh kg^{-1} P_{max} 450 W kg^{-1}		
SiNW* solar cell/SC	$M_{an\text{-}ph}$ PEDOT:PSS /SiNW/n-doped Si $M_{ce\text{-}ph}$ Ag M_{ES+}, M_{ES-} graphene	EL_{ES} H_2SO_4	C_s 16 mF cm^{-2} C% 90% @10000 cycles	η_{con} 12.4 η_{tot} 2.9	19
Perovskite solar cell /SC	$M_{an\text{-}ph}$ c-TiO_2/m-TiO_2 $M_{ce\text{-}ph}$ nanocarbon M_{ES+}, M_{ES-} nanocarbon	EL_{ph} $CsPbBr_3$ EL_{ES} SiO_2 gel	C_s 38 mF cm^{-2} E_{max} 10 µWh cm^{-2} P_{max} 480 µW cm^{-2}	η_{con} 5.1	20
Perovskite solar cell/SC	$M_{an\text{-}ph}$ c-TiO_2/m-TiO_2 $M_{ce\text{-}ph}$ nanocarbon M_{ES+}, M_{ES-} nanocarbon	EL_{ph} $CH_3NH_3PbI_3$ EL_{ES} PVA/H_3PO_4 gel	C_s 12.5 mF cm^{-2} C% 85%@3000 cycle	η_{con} 7.1	21
Perovskite solar cell/SC	M_{ES+}, M_{ES-} carbon/PTFE	EL_{ph} $CsPbI_{3-x}Br_x$ Spiro-MeOTAD/LiTFSI/FK209/tBP EL_{ES} $PYR_{14}TFSI$/TEGDME	C_s 390 mF cm^{-2} Q 360 mC cm^{-2} E_{max} 0.5 mWh cm^{-2} P_{max} 68.4 mW cm^{-2}	—	22
Light-assisted SC	M_{SC} WO_3	H_2SO_4 pH 0	C_s 7.5 mF cm^{-2}	—	23
Light-assisted SC	M_{SC} eumelanin	$NaCH_3COO_{(aq)}$ pH 5.5	C_s 5.3 mF cm^{-2} E_{max} 52 mJ g^{-1} P_{max} 5.9 Wg^{-1} C% 96% @3000 cycles Q%* 103% @3000 cycles	η_{tot} 0.6 (see note below)	This work

Device structure
PSB: Photovoltaically Self-charging Battery
DSSC: Dye Sensitized Solar Cell
SC: Supercapacitor
OPV: Organic Photovoltaic cell
P3HT/PCBM: poly(3-hexylthiophene)/phenyl-C61-butyric acid methyl ester
LIB: Lithium Ion Battery
RFB: Redox Flow Battery
SiNW: Silicon NanoWire
Materials
$M_{an\text{-}ph}$: Material for photoanode
$M_{ce\text{-}ph}$: Material for counter electrode of solar cell
M_{ES+}: Material for the positive electrode of energy storage unit
M_{ES-}: Material for the negative electrode of energy storage unit
N719: Di-tetrabutylammonium *cis*-bis(isothiocyanato)bis(2,2′-bipyridyl-4,4′-dicarboxylato) ruthenium(II) (dye)

N749: cis-bis(isothiocyanato)bis(2,2-bipyridyl-4,4-dicarboxylato)-ruthenium(II)-bis-tetrabutylammonium (dye)
N3: Cis-bis(isothiocyanato)bis(2,2′-bipyridyl-4,4′-dicarboxylato) ruthenium(II) (dye)
CNT: Carbon NanoTube
PC61BM: [6,6]-phenyl-C61-butyric acid methyl ester
PProDOT-Et_2: poly(3,3-diethyl-3,4-dihydro-2Hthieno-[3,4-b][1,4]dioxepine)
PaNi: polyaniline
PEDOT: poly(3,4-ethylenedioxythiophene)
PSS: poly(styrenesulfonate)
PVDF: polyvinylidene fluoride
Z907: Ru(2,2'bipyridyl-4,4'-dicarboxylic acid)(4,4'-dinonyl-2,2'bipyridine)$(NCS)_2$
c-TiO_2: compact-TiO_2
m-TiO_2: mesoporous-TiO_2
PTFE: polytetrafluoroethylene
<u>Electrolytes</u>
EL_{ph}: solar cell electrolyte
EL_{ES}: energy storage electrolyte
EL_{ca}: electrolyte for cathode
EL_{an}: electrolyte for anode
PC: propylene carbonate
tBP: 4-tertbutylpyridine
MPN: 3-methoxypropionitrile
PVA: poly(vinyl alcohol)
DMPII: dimethyl-3-n-propylimidazolium iodide
GNCS: guanidinium thiocyanate
DMII: 1,3-dimethylimidazolium iodide
DMFc: bis(pentamethylcyclopentadienyl)iron
BmimI: 1-butyl-3-methylimidazolium Iodide (ionic liquid)
PVDF-co-HFP: poly(vinylidene fluoride-co-hexa-fluoropropene)
Spiro-MeOTAD: 2,2′,7,7′-tetrakis(N,N-di-p-methoxyphenylamine)-9,9-spirobifluorene
TMAI: tetramethylammonium iodide
IPA: isopropanol
PYR_{14}TFSI: N-butyl-N-methyl pyrrolidinium bis(trifluoromethanesulfonyl)imide
TEGDME: tetraethylene glycol dimethyl ether
LiTFSI: bis(trifluoromethylsulfonyl)imide lithium salt
FK209: tris(2-(1H-pyrazol-1-yl)-4-tertbutylpyridine)-cobalt (III) tris(bis (trifluoromethylsulfonyl)imide)
<u>Energy storage performance</u>
Q_{ch}: charging capacity
Q_{dis}: discharging capacity
C_s: specific capacitance
E_{max}: maximum energy density
P_{max}: maximum power density
Q: capacity
C%: capacitance retention
Q%: capacity retention
<u>Efficiency</u>
η_{tot} overall (energy conversion and storage) efficiency
$\eta_{con:}$ photon-to-electrical energy conversion efficiency
$\eta_{stor:}$ energy storage efficiency

In this work, the total energy conversion and storage efficiency has been calculated using the equation:

$$\eta = \frac{P_{out}}{P_{input}} = \frac{Maximum\ power\ density\ calculated\ during\ discharge\ per\ unit\ area}{Incident\ solar\ power\ density} = \frac{0.59\ mW\ cm^{-2}}{100\ mW\ cm^{-2}} = 0.6\%$$

The maximum power density has been calculated using $P_{max} = \frac{V_{Max}^2}{4\ ESR\ \mathrm{A}}$, where V_{max} is the upper limit of the potential while discharging, ESR is the equivalent series resistance and A is the electrode active area.

Table S2. Capacity and capacitance of DHI- and DHI/DHICA-melanin on carbon paper, extracted from the cathodic currents in the cyclic voltammograms in Figure S1.

Sample	Condition	Cycle number	Capacity ($mC\ cm^{-2}$)	Capacitance ($mF\ cm^{-2}$)
DHI-melanin	Dark	2	2.3	3.2
		4	2.2	3.7
		6	2.3	3.8
	Light	8	2.6	4.9
		10	2.6	4.8
		12	2.7	5.1
		14	2.8	5.2
		16	2.8	5.2
		18	2.8	5.2
		20	2.7	5.1
		22	2.8	5.3
	Dark	24	2.5	4.3
		26	2.4	4.5
		28	2.3	4.3
		30	2.3	4.2

		32	2.3	4.2
		34	2.3	4.3
		36	2.3	4.2
DHI/DHICA-melanin	Dark	2	1.7	2.7
		4	1.8	3.0
		6	1.8	3.1
	Light	8	2.0	3.4
		10	2.0	3.6
		12	2.1	3.8
		14	2.1	3.8
		16	2.1	3.9
		18	2.1	3.8
		20	2.1	3.9
		22	2.1	3.8
	Dark	24	1.8	3.4
		26	1.7	3.2
		28	1.8	3.2
		30	1.8	3.3
		32	1.8	3.3

		34	1.8	3.2
		36	1.7	3.2

Table S3. Average capacity and capacitance calculated for steps lasting for 1000 cycles each in galvanostatic results of melanin-supercapacitor on carbon paper (Figure 2 and 3). Protocol of acquisition: dark → light → 40 min irradiation (no bias) → light → dark → light, each for 1000 cycles.

Sample	Condition	Cycles where the average values are calculated	Capacity during charging ($\mu C\ cm^{-2}$)	Capacity during discharging ($\mu C\ cm^{-2}$)	Capacitance ($\mu F\ cm^{-2}$)
DHI-melanin	Dark	(0-1000)	35	35	121
	Light	(1001-2000)	32	33	115
	Light	(2001-3000)	40	41	127
	Dark	(3001-4000)	37	38	116
	Light	(4001-5000)	39	39	119
DHI/DHICA-melanin	Dark	(0-1000)	20	20	67
	Light	(1001-2000)	20	20	67
	Light	(2001-3000)	21	21	71
	Dark	(3001-4000)	20	20	68
	Light	(4001-5000)	20	20	67

Table S4. Capacity and capacitance change of eumelanin on carbon paper during galvanostatic measurements. The comparison is made for every 1000 cycles (Figures 2 and 3).

Conditions	DHI-melanin		DHI/DHICA -melanin	
	Capacity change	Capacitance change	Capacity change	Capacitance change
Dark	-20%	-12%	-28%	-12%
Light	-9%	-13%	-10%	-6%
Light	-8%	-3%	-10%	-2%
Dark	-2%	-2%	-3%	-2%
Light	+5%	+4%	-3%	+ 1%

Table S5. Fitting parameters of the equivalent circuit of both DHI- and DHI/DHICA-melanin in the frequency range 2 kHz -82 Hz (see also Figure 2 and Figure 3 in the main file).

Fitting parameters	DHI-melanin		DHI/DHICA-melanin	
	Dark	Light	Dark	Light
$R_{tot} = R_u + R_{ct}$ (Ohm)	22.0	18.6	20.3	17.9
Q ($mF.s^{n-1}$)	0.8	1.2	0.4	0.6
n	0.7	0.6	0.7	0.7

References

1. Hauch, A.; Georg, A.; Krašovec, U. O.; Orel, B., Photovoltaically self-charging battery. *Journal of the Electrochemical Society* **2002,** *149* (9), A1208-A1211.

2. Chen, H. W.; Hsu, C. Y.; Chen, J. G.; Lee, K. M.; Wang, C. C.; Huang, K. C.; Ho, K. C., Plastic dye-sensitized photo-supercapacitor using electrophoretic deposition and compression methods. *Journal of Power Sources* **2010,** *195* (18), 6225-6231.

3. Hsu, C. Y.; Chen, H. W.; Lee, K. M.; Hu, C. W.; Ho, K. C., A dye-sensitized photo-supercapacitor based on PProDOT-Et2 thick films. *Journal of Power Sources* **2010,** *195* (18), 6232-6238.

4. Bae, J.; Park, Y. J.; Lee, M.; Cha, S. N.; Choi, Y. J.; Lee, C. S.; Kim, J. M.; Wang, Z. L., Single‐fiber‐based hybridization of energy converters and storage units using graphene as electrodes. *Advanced materials* **2011,** *23* (30), 3446-3449.

5. Wee, G.; Salim, T.; Lam, Y. M.; Mhaisalkar, S. G.; Srinivasan, M., Printable photo-supercapacitor using single-walled carbon nanotubes. *Energy & Environmental Science* **2011,** *4* (2), 413-416.

6. Chen, T.; Qiu, L.; Yang, Z.; Cai, Z.; Ren, J.; Li, H.; Lin, H.; Sun, X.; Peng, H., An integrated "energy wire" for both photoelectric conversion and energy storage. *Angewandte Chemie International Edition* **2012,** *51* (48), 11977-11980.

7. Guo, W.; Xue, X.; Wang, S.; Lin, C.; Wang, Z. L., An integrated power pack of dye-sensitized solar cell and Li battery based on double-sided TiO2 nanotube arrays. *Nano letters* **2012,** *12* (5), 2520-2523.

8. Zhang, X.; Huang, X.; Li, C.; Jiang, H., Dye‐sensitized solar cell with energy storage function through PVDF/ZnO nanocomposite counter electrode. *Advanced Materials* **2013,** *25* (30), 4093-4096.

9. Liu, P.; Cao, Y. l.; Li, G. R.; Gao, X. P.; Ai, X. P.; Yang, H. X., A solar rechargeable flow battery based on photoregeneration of two soluble redox couples. *ChemSusChem* **2013,** *6* (5), 802-806.

10. Fu, Y.; Wu, H.; Ye, S.; Cai, X.; Yu, X.; Hou, S.; Kafafy, H.; Zou, D., Integrated power fiber for energy conversion and storage. *Energy & Environmental Science* **2013,** *6* (3), 805-812.

11. Yang, Z.; Li, L.; Luo, Y.; He, R.; Qiu, L.; Lin, H.; Peng, H., An integrated device for both photoelectric conversion and energy storage based on free-standing and aligned carbon nanotube film. *Journal of Materials Chemistry A* **2013,** *1* (3), 954-958.

12. Xu, J.; Wu, H.; Lu, L.; Leung, S. F.; Chen, D.; Chen, X.; Fan, Z.; Shen, G.; Li, D., Integrated Photo‐supercapacitor Based on Bi‐polar TiO2 Nanotube Arrays with Selective One‐Side Plasma‐Assisted Hydrogenation. *Advanced Functional Materials* **2014,** *24* (13), 1840-1846.

13. Yang, Z.; Deng, J.; Sun, H.; Ren, J.; Pan, S.; Peng, H., Self‐Powered Energy Fiber: Energy Conversion in the Sheath and Storage in the Core. *Advanced Materials* **2014,** *26* (41), 7038-7042.

14. Xu, J.; Chen, Y.; Dai, L., Efficiently photo-charging lithium-ion battery by perovskite solar cell. *Nature communications* **2015,** *6*, 8103.

15. Zhou, F.; Ren, Z.; Zhao, Y.; Shen, X.; Wang, A.; Li, Y. Y.; Surya, C.; Chai, Y., Perovskite photovoltachromic supercapacitor with all-transparent electrodes. *ACS nano* **2016,** *10* (6), 5900-5908.

16. Xu, J.; Ku, Z.; Zhang, Y.; Chao, D.; Fan, H. J., Integrated Photo‐Supercapacitor Based on PEDOT Modified Printable Perovskite Solar Cell. *Advanced Materials Technologies* **2016,** *1* (5), 1600074.

17. Liu, R.; Wang, J.; Sun, T.; Wang, M.; Wu, C.; Zou, H.; Song, T.; Zhang, X.; Lee, S. T.; Wang, Z. L., Silicon nanowire/polymer hybrid solar cell-supercapacitor: a self-charging power unit with a total efficiency of 10.5%. *Nano letters* **2017,** *17* (7), 4240-4247.

18. Vijayakumar, M.; Adduru, J.; Rao, T. N.; Karthik, M., Conversion of Solar Energy into Electrical Energy Storage: Supercapacitor as an Ultrafast Energy‐Storage Device Made from Biodegradable Agar‐Agar as a Novel and Low‐Cost Carbon Precursor. *Global Challenges* **2018**, 1800037.

19. Liu, H.; Li, M.; Kaner, R. B.; Chen, S.; Pei, Q., Monolithically Integrated Self-Charging Power Pack Consisting of a Silicon Nanowire Array/Conductive Polymer Hybrid Solar Cell and a Laser-Scribed Graphene Supercapacitor. *ACS applied materials & interfaces* **2018,** *10* (18), 15609-15615.

20. Liang, J.; Zhu, G.; Wang, C.; Zhao, P.; Wang, Y.; Hu, Y.; Ma, L.; Tie, Z.; Liu, J.; Jin, Z., An all-inorganic perovskite solar capacitor for efficient and stable spontaneous photocharging. *Nano Energy* **2018,** *52*, 239-245.

21. Liang, J.; Zhu, G.; Lu, Z.; Zhao, P.; Wang, C.; Ma, Y.; Xu, Z.; Wang, Y.; Hu, Y.; Ma, L., Integrated perovskite solar capacitors with high energy conversion efficiency and fast photo-charging rate. *Journal of Materials Chemistry A* **2018,** *6* (5), 2047-2052.

22. Intermite, S.; Arbizzani, C.; Soavi, F.; Gholipour, S.; Turren-Cruz, S.-H.; Correa-Baena, J. P.; Saliba, M.; Vlachopoulos, N.; Ali, A. M.; Hagfeldt, A., Perovskite solar cell–electrochemical double layer capacitor interplay. *Electrochimica Acta* **2017,** *258*, 825-833.

23. Zhu M., Huang Y., Huang Y., Pei Z., Xue Q., Li H., Geng H., Zhi C., Capacitance Enhancement in a Semiconductor Nanostructure-Based Supercapacitor by Solar Light and a Self-Powered Supercapacitor–Photodetector System. *Advanced Functional Materials* **2016**, *26*, 4481-4490.